Journal of Power Sources 195 (2010) 6008–6015

Contents lists available at ScienceDirect

Journal of Power Sources

journal homepage: www.elsevier.com/locate/jpowsour

Development of the novel control algorithm for the small proton exchange membrane fuel cell stack without external humidification

Tae-Hoon Kim [a], Sang-Hyun Kim [a], Wook Kim [a], Jong-Hak Lee [a], Kwan-Seok Cho [a], Kyung-Won Park [b], Woojin Choi [a,*]

[a] Department of Electrical Engineering, Soongsil University, 1-1 Sangdo-dong, Dongjak-gu, Seoul 156-743, Republic of Korea
[b] Department of Chemical/Environmental Engineering, Soongsil University, 1-1 Sangdo-dong, Dongjak-gu, Seoul 156-743, Republic of Korea

ARTICLE INFO

Article history:
Received 27 August 2009
Received in revised form
28 November 2009
Accepted 2 December 2009
Available online 11 December 2009

Keywords:
Fuel cell
Water management
Heat management
Dual closed-loop
Purge
Microcontroller

ABSTRACT

Small PEM (proton exchange membrane) fuel cell systems do not require humidification and have great commercialization possibilities. However, methods for controlling small PEM fuel cell stacks have not been clearly established. In this paper, a control method for small PEM fuel cell systems using a dual closed loop with a static feed-forward structure is defined and realized using a microcontroller. The fundamental elements that need to be controlled in fuel cell systems include the supply of air and hydrogen, water management inside the stack, and heat management of the stack. For small PEM fuel cell stacks operated without a separate humidifier, fans are essential for air supply, heat management, and water management of the stack. A purge valve discharges surplus water from the stack. The proposed method controls the fan using a dual closed loop with a static feed-forward structure, thereby improving system efficiency and operation stability. The validity of the proposed method is confirmed by experiments using a 150-W PEM fuel cell stack. We expect the proposed algorithm to be widely used for controlling small PEM fuel cell stacks.

1. Introduction

Compared to other types of fuel cells, PEM (proton exchange membrane) fuel cells operate at a relatively low temperature with high efficiency and have a smaller volume. Many studies on PEM fuel cells have been conducted to investigate their applications in portable electronics, residential power generation, and fuel cell vehicles [1]. PEM fuel cell systems are composed of a fuel cell stack that generates electricity by reacting with the fuel gases and the BOP (balance of plant) that assists the stack operation by controlling the fuel supply, pressure, temperature, and humidity.

In small fuel cell systems, the role of the BOP is to consume minimal power while guaranteeing stable operation of the stack. Its main functions include supply of necessary air and hydrogen, heat management in the stack, and water management for the MEA (membrane electrode assembly). Hydrogen is supplied directly to the stack from a compressed gas cylinder through a pressure regulator. The hydrogen flow rate is decided by instantaneous pressure differences in the stack caused by load changes. Therefore, small PEM fuel systems do not require a separate device to control the hydrogen flow. The use of a pump or motor is not recommended because it increases the overall system size, price, and BOP power consumption. For the same reasons, it is not economically feasible to use an external humidifier for water management. The air needed for reaction and cooling is supplied by a fan without a separate humidifying device. Surplus water in the stack is discharged through a purge valve. Therefore, an economically feasible and efficient method of operation is to manage water and heat by appropriate control of the fan and the purge valve.

Recently, several studies on fuel cell power systems have been published [2–6] showing their potential as power sources for portable electronics. Urbani et al. [2] designed, manufactured, and tested an air-breathing 10-cell PEFC (polymer electrolyte fuel cell) stack; they were able to operate a 12-W DVD player for 100 h without sensitive losses in performance. Dundar et al. [3] built a 70-W fuel cell stack, presented a systematic design procedure for portable applications, and comprehensively analyzed the effects of variables such as reactant gas humidification, cooling, fuel supply, and temperature. However, in the proposed system, a humidifier is used at the input side of the cathode for water management in the membrane, and therefore, the system becomes complicated. Hebling et al. [4] developed several fuel cell systems with power ratings from 10 to 180-W and implemented digital control algo-

* Corresponding author. Tel.: +82 2 820 0652; fax: +82 2 817 7961.
E-mail addresses: hoon7147@hotmail.com (T.-H. Kim), hyun714@hotmail.com (S.-H. Kim), kormook@hotmail.com (W. Kim), jonghak123@hotmail.com (J.-H. Lee), pandu99@ssu.ac.kr (K.-S. Cho), kwpark@ssu.ac.kr (K.-W. Park), cwj777@ssu.ac.kr (W. Choi).

0378-7753/$ – see front matter © 2009 Elsevier B.V. All rights reserved.
doi:10.1016/j.jpowsour.2009.12.009

Nomenclature

A_{st}	exposed surface area of fuel cell stack (m^2)
c_p	specific heat of air at constant pressure ($J\,mol^{-1}\,K^{-1}$)
F	Faraday constant (coulomb mol^{-1})
g	gravity acceleration ($m\,s^{-2}$)
h	convection heat transfer coefficient ($W\,m^{-2}\,K^{-1}$)
h_r	radiation heat transfer coefficient ($W\,m^{-2}\,K^{-1}$)
I_{st}	current of fuel cell stack (A)
k	thermal conductivity ($W\,m^{-1}\,K^{-1}$)
L	height of the stack (m)
$\dot{m}_{reac,air}$	air flow rate necessary for reaction ($mol\,s^{-1}$)
$\dot{m}_{cool,air}$	air flow rate necessary for cooling ($mol\,s^{-1}$)
$\dot{m}_{ref}$	air flow rate necessary for operation of fuel cell stack ($mol\,s^{-1}$)
Nu_L	Nusselt number
n_{cell}	number of cells
P_e	power of fuel cell stack (W)
P_{ent}	total pressure of entrance air (kPa)
P_{exit}	total pressure of exit air (kPa)
P_{sat}	saturated vapor pressure (kPa)
P_{Went}	water vapor pressure at the entrance (kPa)
Pr	Prandtl number
Pm	exposed surface perimeter of fuel cell stack (m)
Q_{cool}	cooling rate to be removed with forced cooling (W)
Q_{reac}	cooling rate by the flow which participates in reaction (W)
Q_{conv}	cooling rate by the natural convection (W)
Q_{rad}	cooling rate by the natural radiation (W)
Q_{st}	heating rate of fuel cell stack (W)
Q_{dis}	natural heat dissipation (W)
Ra_L	Rayleigh number
$T_{air,exit}$	exit air temperature (K)
T_{st}	stack surface temperature (K)
T_o	temperature of the surrounding walls (K)
ΔT_{reac}	difference of temperature of entrance and exit in reaction air (K)
ΔT_{cool}	difference of temperature of entrance and exit in cooling air (K)
t_{purge}	purge cycle of solenoid valve (s)
V_{cell}	voltage of stack per cell (V)
a,b,c,d,e,f	empirical coefficients of saturated vapor pressure

Greek symbols

α	thermal diffusivity ($m^2\,s^{-1}$)
β	thermal expansion coefficient (K^{-1})
ε	emissivity
λ_{air}	air stoichiometry
υ	kinematic viscosity ($m^2\,s^{-1}$)
σ	Stefan–Boltzmann constant ($W\,m^{-2}\,K^{-4}$)
Ψ	water coefficient of entrance air

rithms in a digital microprocessor to achieve quick responses to changes in the operating conditions. The hydrogen closed loop achieved current density rates up to 550 mA cm^{-2} and a fuel utilization coefficient greater than 0.99 after startup. Vega-Leal et al. [5] focused on the physical implementation of the digital controller for the fuel cell stack. The proposed system includes three control loops assigned to the control of oxygen flow, hydrogen flow, and temperature. Wilhelm et al. [6] developed a PEM-fuel-cell-powered mobile robot. The authors investigated the feasibility of using the robot in a university-level course and succeeded in demonstrating the potential of the technology.

Büchi and Srinivasan [7] presented the results of a study on water management for small PEM fuel cell stacks without external humidifiers. They developed a model for PEM fuel cell operation with internal humidification of the gases and investigated the range of operating conditions for a PEM fuel cell using dry H_2/air. It was found that MEA water management could be achieved by maintaining the relative humidity of the exit air between 80% and 100%. Therefore, it should be possible to control small self-humidified stacks by controlling the air flow for fuel and cooling. However, no detailed control algorithm was provided in the article.

Several other studies were conducted on the topic of water management in small self-humidified fuel cell stacks [8–10], and they provide excellent insights into water management. However, practical control algorithm for the stable and reliable operation of small PEM fuel cell systems based on comprehensive analysis of water management was not clearly established in the previously conducted studies.

In this study, we present a novel BOP control method for small self-humidified stacks. The proposed method successfully controls the overall system by calculating and supplying the amount of fuel that allows water and heat in the stack to achieve equilibrium. Using this method, high system efficiency and operating reliability can be achieved. The feasibility of the method was confirmed by experiments using a 150-W PEM fuel cell stack.

2. Description of control concept

2.1. Fuel supply and water management

The air flow rate to be supplied for electrochemical reactions in the fuel cell stack $\dot{m}_{reac,air}$ is calculated as shown in Eq. (1) considering the ratio of oxygen in the atmosphere.

$$\dot{m}_{reac,air} = \frac{P_e}{4FV_{cell}} \times \frac{1}{0.21} \tag{1}$$

where P_e is the power of the fuel cell stack, V_{cell} is the voltage per cell of the stack, and F is the Faraday constant.

However, if the value obtained from Eq. (1) is used without modification, as oxygen is consumed by the reaction, the voltage loss from the reduced partial oxygen pressure becomes larger, and fuel supply may become difficult because of the water formed in the channel. Therefore, in practical applications, a stoichiometric variable λ_{air} that has a larger value than that defined by Eq. (1) should be introduced. According to previous studies, the optimal stoichiometry of air is approximately 2–2.4 [11]. In a small PEM fuel cell system with no external humidifier, the reliability of the water management in the MEA can be maintained by appropriate stoichiometric configuration according to the stack conditions.

For the MEA in the PEM fuel cell stack to have sufficient water, the relative humidity of the cathode exit air should be between 80% and 100%, and this can be achieved by selecting an appropriate stoichiometry for the air flow rate according to the operation temperature of the stack [7]. Thus, by considering the water coefficient of entrance air (atmosphere) Ψ in Eq. (3) and substituting it into Eq. (2), a stoichiometry that satisfies the water condition in the stack can be calculated.

$$\lambda_{air} = \frac{0.210(P_{sat} - P_{exit})}{\Psi P_{exit} - (1+\Psi)P_{sat}} \tag{2}$$

$$\Psi = \frac{P_{Went}}{P_{ent} - P_{Went}} \tag{3}$$

where P_{exit} is the total pressure of the exit air, P_{ent} is the total pressure of the entrance air, P_{Went} is the water vapor pressure at the entrance, and P_{sat} is the saturated vapor pressure according to exit-air temperature. In the temperature ($T_{air,exit}$) range from 273.15 to

373.15 K, the following empirical equation can be used [12]:

$$P_{sat} = f(T_{air,exit}) = e^{\alpha T^{-1}+b+cT+dT^2+eT^3+f\ln(T)} \quad (4)$$

where $a = -5880.2206$, $b = 1.3914993$, $c = -0.048640239$, $d = 0.41764768 \times 10^{-4}$, $e = -0.14452093 \times 10^{-7}$, and $f = 6.5459673$.

Therefore, taking the stoichiometry into account, the air flow rate necessary for the stack reaction is calculated as shown in Eq. (5).

$$\dot{m}_{reac,air} = \frac{P_e}{4FV_{cell}} \times \frac{1}{0.21} \times \lambda_{air} \quad (5)$$

2.2. Heat management

Heat management of small PEM fuel cell stacks is mainly accomplished by supplying the fuel air $\dot{m}_{reac,air}$ and cooling air $\dot{m}_{cool,air}$ together through the fan. The heating rate that is created by the operation of the stack, Q_{st}, should be equal to the sum of the cooling rate from forced cooling by the fan (Q_{cool}), natural heat dissipation (radiation + convection) ($\sum Q_{dis}$), and cooling rate from the flow that participates in the electrochemical reaction (Q_{reac}). This relation is shown in Eq. (6).

$$Q_{st} = Q_{cool} + \sum Q_{dis} + Q_{reac} \quad (6)$$

Assuming that the water formed through electrochemical reactions in the fuel cell is completely discharged in the vapor state and that the reaction enthalpy is entirely converted to electric energy, the voltage of the fuel cell is 1.25 V (lower heating value basis). The heating rate of the stack can then be expressed as follows using the current of the fuel cell stack, I_{st}, and the number of cells, n_{cell} [13].

$$Q_{st} = (1.25 - V_{cell}) I_{st} n_{cell} \quad (7)$$

Natural heat dissipations from the stack are classified into convection Q_{conv} and radiation Q_{rad}, as described in Eq. (8) [14].

$$\sum Q_{dis} = Q_{conv} + Q_{rad} \quad (8)$$

The cooling rate from natural convection, Q_{conv}, can be calculated using Eq. (9).

$$Q_{conv} = hA_{st}(T_{st} - T_0) \quad (9)$$

where h is the convection heat transfer coefficient and is a function of the Nusselt number, Nu_L. The value of h can be calculated using Eq. (10).

$$h = \frac{k}{L} Nu_L \quad (10)$$

The Nusselt number changes with the shape of the heating element; it can be calculated by Eq. (11) in the case of vertical plates, by Eq. (12) in the case of the upper surface of horizontal plates, and by Eq. (13) in the case of the lower surface of the fuel cell stack [12,14].

$$Nu_L = \left\{ 0.825 + \frac{0.387 Ra_L^{1/6}}{[1 + (0.5/Pr)^{9/16}]^{8/27}} \right\}^2 \quad (11)$$

where $Ra_L = g\beta(T_{st} - T_0)L^3/\upsilon\alpha$, $Pr = \upsilon/\alpha$.

$$Nu_L = 0.54 Ra_L^{1/4} \quad (10^4 \le Ra_L \le 10^7) \quad (12)$$

$$Nu_L = 0.27 Ra_L^{1/4} \quad (10^5 \le Ra_L \le 10^{10}) \quad (13)$$

where $L = A_{st}/Pm$.

The cooling rate from natural radiation Q_{rad}, can be expressed as Eq. (14).

$$Q_{rad} = h_r A_{st}(T_{st} - T_o) \quad (14)$$

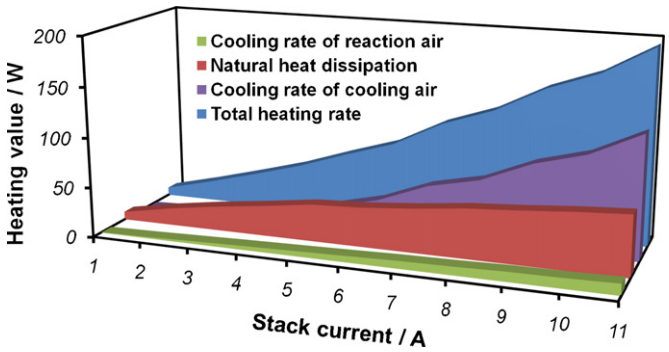

Fig. 1. Various heating and cooling rates in 150-W PEM fuel cell stack.

where h_r is the radiation heat transfer coefficient calculated using Eq. (15).

$$h_r = \varepsilon\sigma(T_{st} + T_o)(T_{st}^2 + T_o^2) \quad (15)$$

Air used as fuel also participates in the cooling of the stack, and the cooling rate is as follows:

$$Q_{reac} = \dot{m}_{reac,air} c_p \Delta T_{reac} \quad (16)$$

The forced cooling rate from air supplied by the fan is as follows.

$$Q_{cool} = \dot{m}_{cool,air} c_p \Delta T_{cool} \quad (17)$$

where c_p is the specific heat of air at constant pressure, ΔT_{reac} is the temperature difference in the reaction air, and ΔT_{cool} is the temperature difference in the cooling air.

Thus, the heating rate of the stack, cooling rate of the reaction air, and heat dissipation by natural convection and radiation can be calculated using Eqs. (6)–(17) and plotted against the stack current, as shown in Fig. 1. The total air flow rate for the cooling of the 150-W PEM fuel cell stack supplied by the fan can be calculated using Eq. (18).

$$\dot{m}_{cool,air} = \frac{Q_{st} - \sum Q_{dis} - Q_{reac}}{c_p \Delta T_{cool}} \quad (18)$$

2.3. Optimal selection and control of BOP

2.3.1. Optimal selection of BOP

Since the fan consumes most of the BOP power in small fuel cell systems, the efficiency and stability of the overall system can be improved by optimal selection and control of the fan. Conditions for selecting the fan include efficiency, ability to be controlled by a microcontroller, ability to be operated without sparks, and reliability. In addition, the fan must have enough capacity to supply the required flow. To select an optimal fan, the air flow rate necessary for operation of the fuel cell stack must first be calculated. This can be calculated as the sum of the air flow rate necessary to carry out the reaction shown in Eq. (5) and the air flow rate necessary to achieve cooling according to Eq. (18). As shown in Fig. 2, the calculated air flow rate matched the experimental air flow rate during steady-state operation. However, the relationship between the required air flow rate and the stack current is not linear and online calculation of the value is not efficient because of the long calculation time required by the microcontroller. Moreover, it presumes the use of multiple temperature and humidity sensors. Therefore, in this study, we calculated the air flow rate required for each stack current, $\dot{m}_{ref}$, in advance and carried out curve-fitting to convert the values into the polynomial expression shown in Eq. (19).

$$\dot{m}_{ref} = -0.0004 I_{st}^3 + 0.00062 I_{st}^2 + 0.0207 I_{st} - 0.0124 \quad (19)$$

Using the maximum air flow rate calculated above, we selected an optimal fan for the supply of air in the fuel cell system. First,

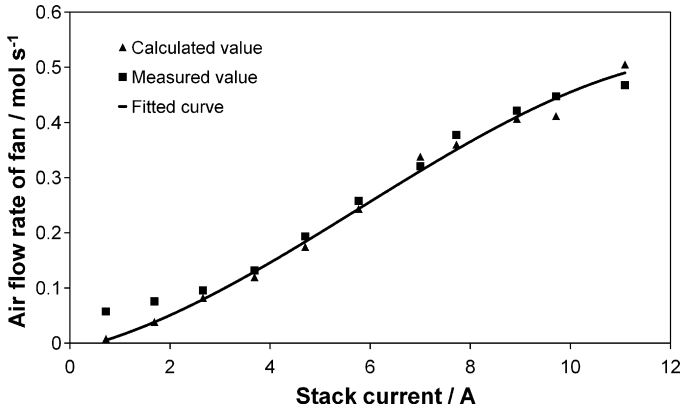

Fig. 2. Calculated and measured air flow rate and fitted curve.

after finding the system resistance curve that gives the static pressure according to air flow rate, we compared the curve with the performance curve of the fan provided by the manufacturer. The intersection of these two curves gives the operating point of the fan in the fuel cell system. Therefore, when the fan is operated at its rated value, the total air flow rate necessary for the fuel cell stack must be satisfied at the operating point. The power consumption must also be small.

Fig. 3 shows the system resistance curve of the 150-W PEM fuel cell system used in the experiment and the performance curves of three fans. From Eq. (19), the maximum air flow rate required for operation of the small PEM fuel cell stack in this study is approximately 0.68 $m^3\ min^{-1}$ at a current of 10 A. Because two fans are attached to the left and right of the stack for uniform cooling, the rated flow of each fan should be approximately 0.17 $m^3\ min^{-1}$. Of the three fans shown in Fig. 3, fan 3 supplies approximately 0.17 $m^3\ min^{-1}$ at the operating point but has a high power consumption of 2.52-W. Fan 2 exhibits the lowest power consumption of 1.68-W but cannot supply the necessary air flow rate. Thus, we selected fan 1, which can supply an air flow rate of 0.17 $m^3\ min^{-1}$ and has a low power consumption of 2.40-W.

The purge valve for the discharge of surplus water should also have a low power requirement. It must withstand the flow of water discharged at the operating pressure. We used a small solenoid valve requiring 2.0-W of power and appropriate for a flow of 13 l min^{-1} at 25 psig.

2.3.2. Control of BOP

Speed control of the fan is mandatory to reduce the average power consumption and to quickly supply the standard air flow

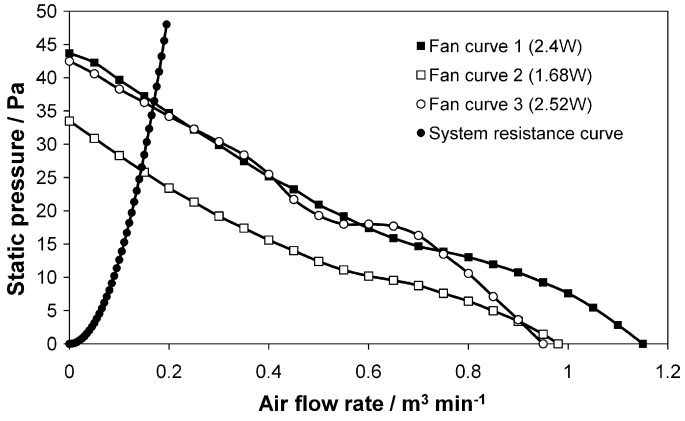

Fig. 3. Performance curves of fans and system resistance curve.

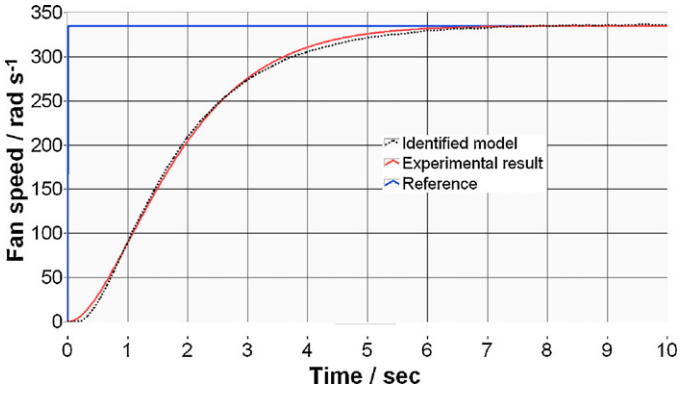

Fig. 4. Step response of fan.

Table 1
Extracted fan parameters.

Parameter	Value
Gain, K	67.3
Damping ratio, ζ	1.12
Natural frequency, ω_n	1.12

rate. There are various methods for fan speed control. To perform PI (proportional-integral) control, we used the internal PWM (pulse width modulation) method because it has high accuracy, a relatively low noise level, no power loss from external constituents, and high efficiency. The normal transfer function of the angular velocity against the terminal voltage of a BLDC (brushless direct current) motor is expressed in Eq. (20) [15]. This transfer function of the fan must be known to design the speed controller of the fan.

$$G(s) = \frac{\omega_m(s)}{V(s)} = \frac{K\omega_n^2}{s^2 + 2\zeta\omega_n s + \omega_n^2} \tag{20}$$

We estimated the transfer function using LabVIEW 8.6 with System Identification Toolkit 4.0 after performing an experiment on fan step response. Fig. 4 shows the response characteristics of the fan against step voltage input, and the response from the estimated model corresponds to the experimental result. As shown in Fig. 4, the fan showed an overdamped characteristic with no overshoot. Table 1 summarizes the extracted fan parameters.

The step response time of the system is approximately 6 s and such a slow transient response delays the supply of necessary air. To improve the transient response of the BLDC fan, a PI controller defined in Eq. (21) [16] was used for the inner control loop, as shown in Fig. 5. The controller was designed to meet a suitable phase margin (45° in this case) at the gain-crossover frequency to guarantee system stability. Fig. 6 shows bode plots of the fan with open-loop and closed-loop control. The proportional and integral gains of the PI controller for the inner control loop are listed in Table 2.

$$C(s) = K_p^{in} + \frac{K_i^{in}}{s} \tag{21}$$

Thus, the closed-loop transfer function of the fan can be obtained by multiplying Eqs. (20) and (21) in the frequency domain; the transfer function must be converted to a discrete-time linear transfer function for actual implementation in the microcontroller; this

Table 2
Gain of inner PI controller.

Parameter	Value
Proportional gain, $K^{in}{}_p$	0.12
Integral gain, $K^{in}{}_i$	0.0032

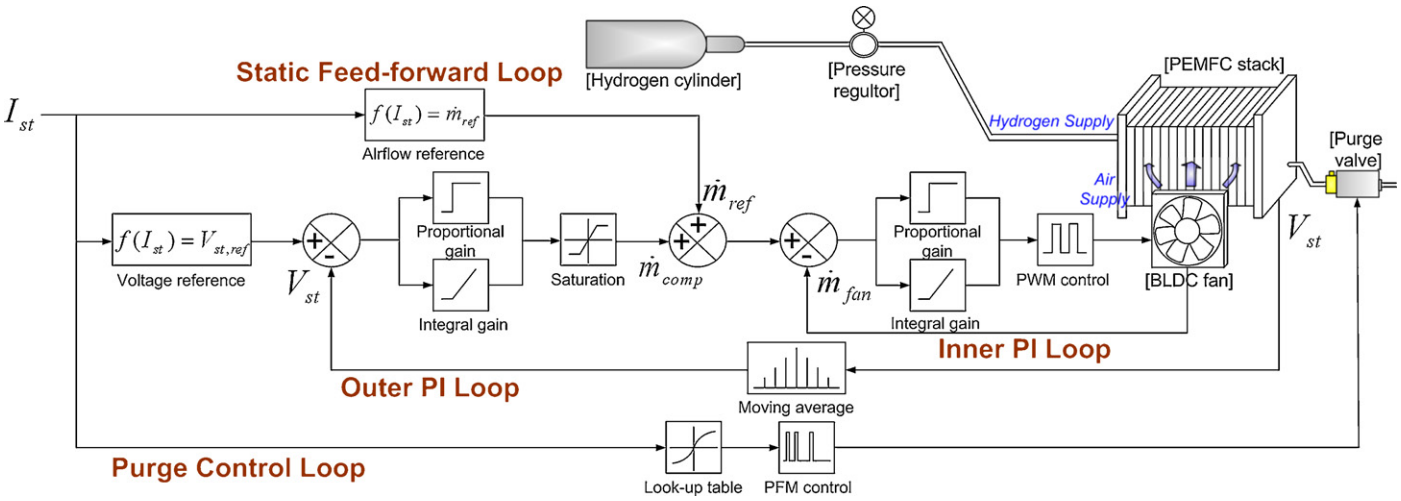

Fig. 5. Block diagram of proposed control algorithm for small PEM fuel cell system.

is done by using bilinear transformation as shown in Eq. (22) [16].

$$H_{CL}(z) = \frac{G(z)C(z)}{1 + G(z)C(z)} = \frac{a_0 z^3 + a_1 z^2 + a_2 z + a_3}{b_0 z^3 + b_1 z^2 + b_2 z + b_3} \tag{22}$$

where

$$a_0 = 0.00035, \quad a_1 = 0.00036, \quad a_2 = -0.00036, \quad a_3 = -0.00035$$

$$b_0 = 1, \quad b_1 = -2.97004, \quad b_2 = 2.94064, \quad b_3 = -0.97095$$

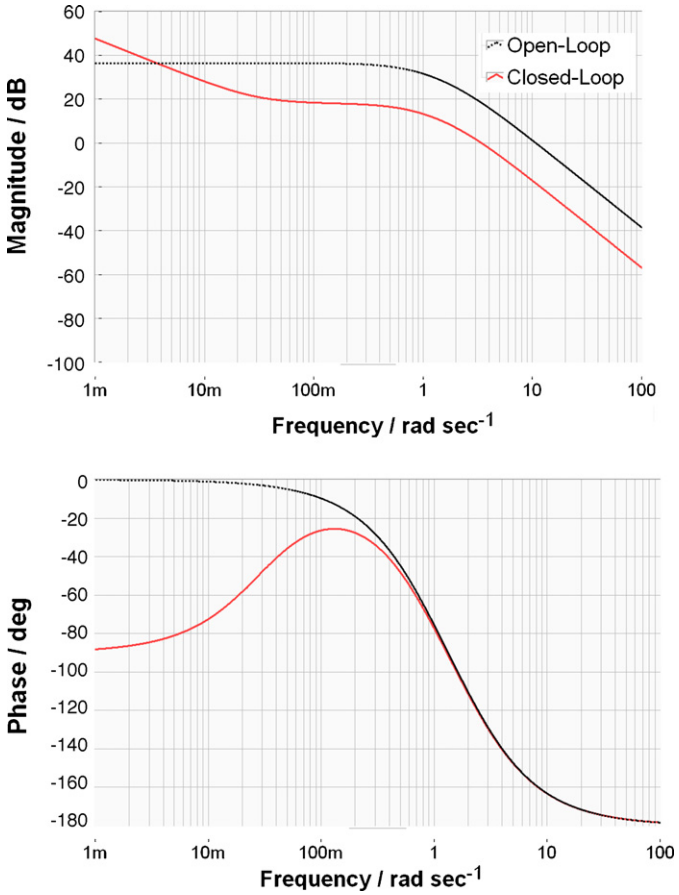

Fig. 6. Open-loop and closed-loop bode plots of BLDC fan.

The air flow rate necessary for stack reaction and cooling with consideration of the MEA water management can clearly be calculated using Eq. (19) from the stack current. Also, according to the transient response characteristic of the fuel cell stack, the transient response of the voltage has a time delay compared to the response speed of the current when rapid load changes occur. Therefore, the air flow rate calculated using Eq. (19) from the stack current must be static feed-forward controlled, as shown in Fig. 5, for a quicker system response. In addition, the outer control loop that controls the voltage feedback of the fuel cell stack is configured to be 10 times slower than the inner control loop that controls the fan speed. A moving-average method is applied to the feedback voltage to form a loop that is insensitive to noise or instantaneous stack voltage changes.

The outer control loop calculates the difference between the feedback voltage and the stack voltage in the steady state to create a correction term. This term is added to the reference air flow rate generated by the static feed-forward loop. Accordingly, the reference air flow rate calculated with the stack current by the static feed-forward control loop is supplied quickly to the stack through the inner control loop to obtain the necessary fuel supply and achieve heat management. Feedback of the stack voltage allows operation of the fuel cell stack at the optimal operating point via the correction supplied by the outer loop. Table 3 lists the PI controller gain for the outer control loop.

However, in small PEM fuel cell systems, because water management in the MEA is also carried out by controlling the air flow rate using the fan, the flow added or reduced by the outer loop must not influence the water management. The condition for sufficient water in the MEA inside the PEM fuel cell stack is that the relative humidity of the cathode exit air must be kept between 80% and 100%, and this should be maintained even if the flow supplied to the stack by the outer loop is changed. Therefore, if there is a correction for the air flow rate from the outer control loop, the supplied air flow must be limited to prevent the relative humidity at the cathode exit from falling below 80%. Similarly, the minimum air flow rate is the value that prevents the relative humidity at the exit from exceeding 100%. In the outer loop control, limitation of the air flow

Table 3
Gain of outer PI controller.

Parameter	Value
Proportional gain, $K^{out}{}_p$	0.024
Integral gain, $K^{out}{}_i$	2.0e−05

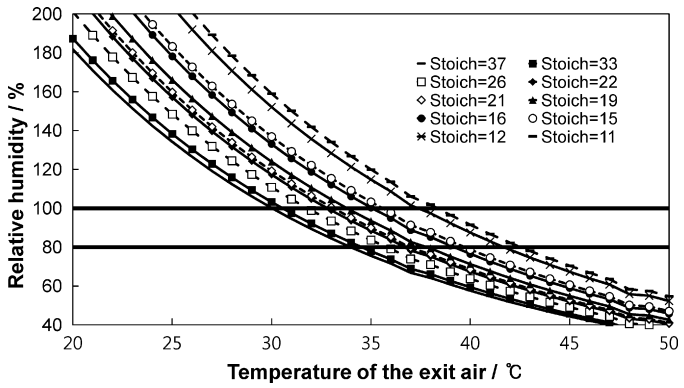

Fig. 7. Relationship of relative humidity and temperature with various stoichiometries.

rate is necessary to satisfy these conditions. Here, since changes in the temperature of the cathode exit air are much slower than changes in the voltage, the influence of temperature change does not need to be considered. Fig. 7 shows the relationships between cathode exit air temperature and relative humidity with various stoichiometries.

On the cathode side of the fuel cell stack, water is formed as a byproduct of the electrochemical reaction, and the amount of water increases linearly as the stack current increases. In the aforementioned control algorithm, the air stoichiometry is selected to keep the relative humidity of the exit air between 80% and 100% to ensure sufficient water circulation in the MEA by electro-osmotic drag and back diffusion. However, when the stack operates in high-current conditions, water formed by the reaction accumulates in the anode because the amount of water from back diffusion becomes larger than that from electro-osmotic drag. Accumulation of surplus water in the anode causes flooding and to prevent this, discharge of water through the purge valve is required [12]. In this study, the optimal purge cycle of the stack giving the best performance under different load conditions is measured experimentally. The purge valve is controlled by an ATmega128 microcontroller via the PFM (pulse frequency modulation) method based on the polynomial expression (Eq. (23)) obtained by curve-fitting, as shown in Fig. 8.

$$t_{purge} = -0.160I_{st}^3 + 3.310I_{st}^2 - 22.43I_{st} + 55.84 \quad (23)$$

3. Experimental

The 150-W PEM fuel cell stack used for the experiment is composed of 24 unit cells and 3 cooling cells. The cell was manufactured by BCS Fuel Cells and has an electrode area of 50 cm^2. Since the use of hydrogen at 99.99% purity is required, high-purity hydrogen stored in a compressed gas cylinder under 100 atm was reduced to 0.2 atm using a pressure regulator before being supplied to the stack. At the end of the anode, a solenoid valve is connected for the purging. Because the system has no separate humidification device, it is appropriate for use as a small power source.

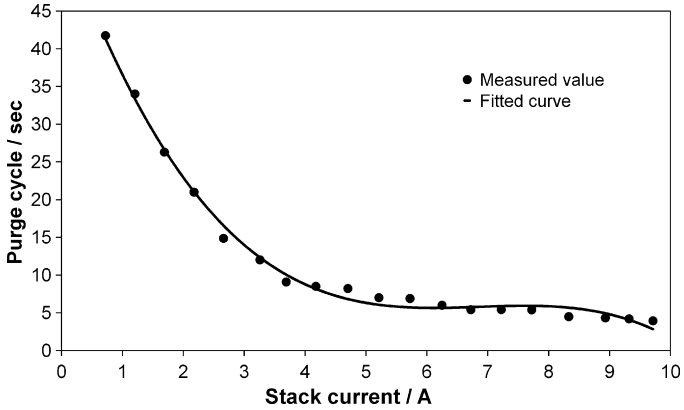

Fig. 8. Optimal purge cycle showing best performance at different load conditions.

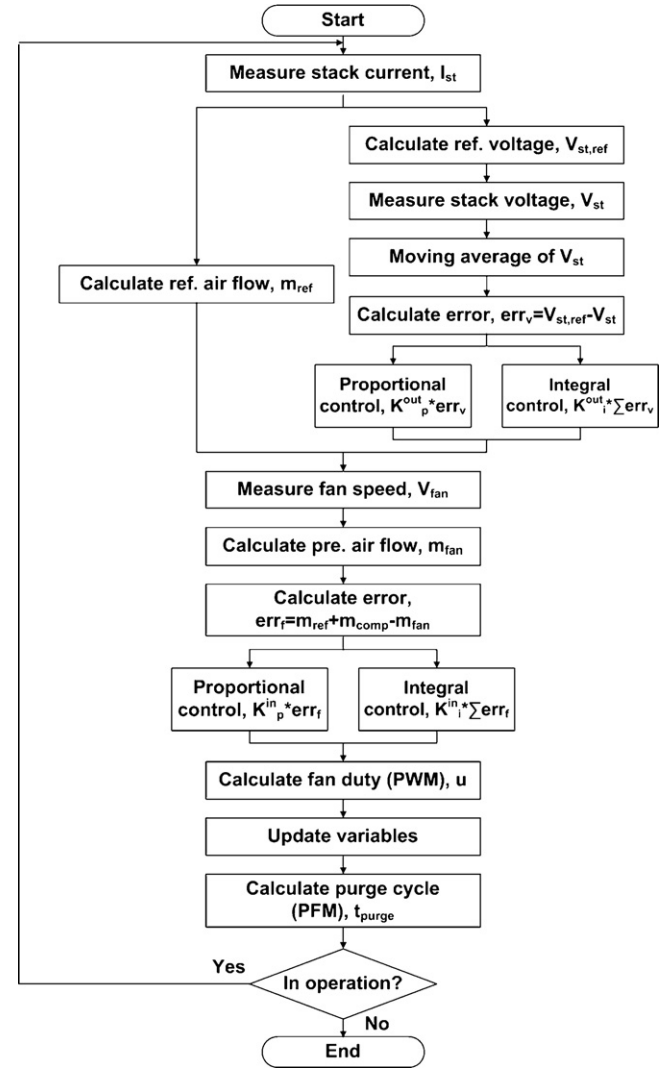

Fig. 9. Flowchart for proposed control algorithm of small PEM fuel cell system.

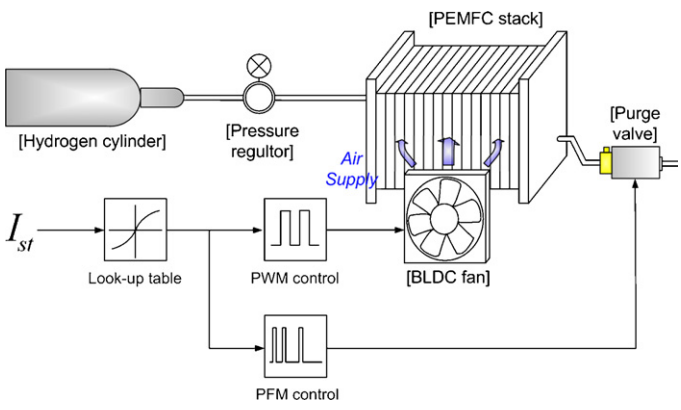

Fig. 10. Control of small PEM fuel cell stack by SFFC using look-up table.

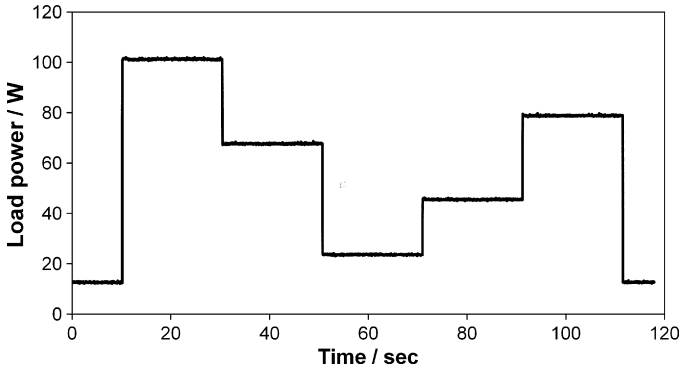

Fig. 11. Power profile applied to fuel cell stack.

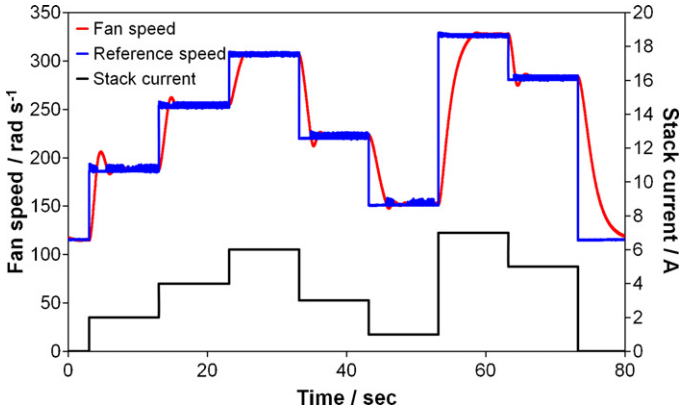

Fig. 12. Dynamic response of BLDC fan with PI controller.

To implement the proposed control algorithm, ATmega128, an 8-bit microcontroller from Atmel, was used to create a control circuit. A sensing circuit, LabVIEW 8.6, and a PCI-6154 were used to record values for the fuel cell stack on a real-time basis. PCI-6154 is a simultaneous sampling multifunction I/O device for PCI bus computers from National Instruments [17]. It is an isolated PCI device featuring four isolated differential 16-bit analog inputs, four isolated 16-bit analog outputs, six DI lines, four DO lines, and two general-purpose 32-bit counter/timers. All A/D converters and D/A converters are capable of handling a max sampling rate of 250 kS s^{-1} for each channel. Fig. 9 shows a flowchart of the proposed control algorithm implemented in the microcontroller. A small 150-W PEM fuel cell system and control circuit were developed and used for the experiment.

To test the performance and efficiency of the developed controller, we compare the conventional SFFC (static feed-forward control) method (Fig. 10) developed using a look-up table [11,18] and the SFFC + DCC (static feed-forward control + dual closed-loop control) method proposed in this paper by performing identical experiments. In the experiments, the 150-W PEM fuel cell stack is loaded according to the power profile shown in Fig. 11.

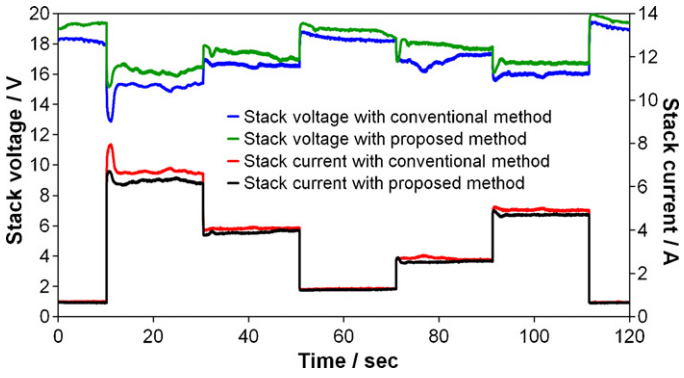

Fig. 13. Voltage and current waveforms of stack for each control method.

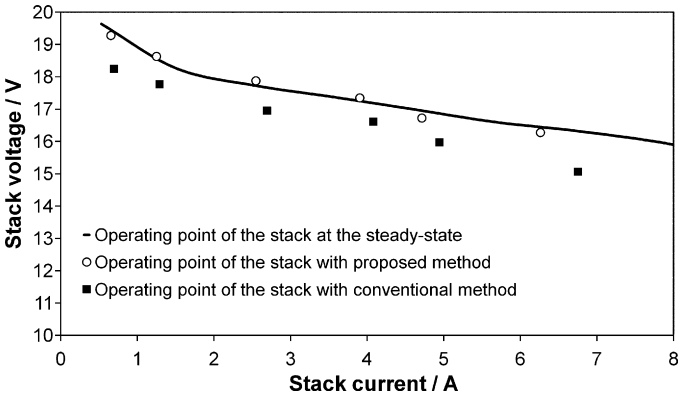

Fig. 14. Comparison of operating points for each control method.

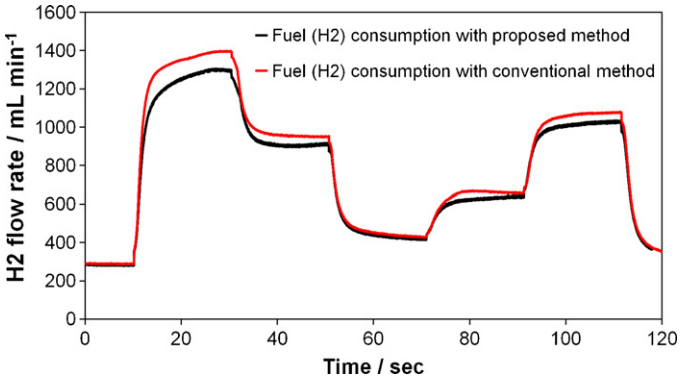

Fig. 15. Hydrogen consumption of stack for each control method.

4. Results and discussion

Fig. 12 shows the dynamic response waveform of the fan controlled by the PI controller. The fan speed that can supply the required air flow rate calculated from the stack current becomes the command value. As can be seen in Fig. 12, the fan satisfactorily follows the command speed. In addition, the comparison of the step response characteristics shown in Figs. 4 and 12 revealed that using the PI controller shortened the time taken to follow the speed command value, and therefore the design of the fan controller was carried out appropriately.

Fig. 13 shows the voltage and current waveforms of the fuel cell stack using the SFFC and SFFC + DCC control methods when the load varies as shown in Fig. 11. As can be seen in Fig. 13, both methods show stable tracking performance as load power changes, but the stack voltage of the proposed method is higher than that of the conventional method. In contrast, the stack current of the proposed method is lower than that of the conventional method. This means that the operating points of the two control methods are different although the same power is extracted from the fuel cell stack, as shown in Fig. 14. Moreover, the fuel consumptions are different as shown in Fig. 15. After applying the power profile for 120 s, the electric energy supplied to the load and the number of moles of hydrogen consumed are 6489 J and 0.0635 mol for the conventional method, and 6475 J and 0.0601 mol for the proposed method, respectively. The average stack efficiency was calculated to

be 42.24% and 44.53%, respectively. Therefore, the proposed control method allows the stack to run at its optimal operating point and improves the fuel-to-power efficiency.

5. Conclusion

A novel dual closed-loop method with a static feed-forward control was proposed in this paper to control a small PEM fuel cell system, and the algorithm was implemented using a microcontroller. The proposed method improved the slow transient response of a fan via inner PI control and supplied the air flow rate calculated from the stack current via static feed-forward control. Any output voltage deviation from the steady-state value can be corrected by feeding it into the additional outer PI controller to generate a correction term for the air flow rate, thereby improving system efficiency and achieving operation stability. The proposed control algorithm is expected to be useful for controlling small fuel cell stacks.

Acknowledgements

This work (research) is financially supported by the Ministry of Knowledge Economy (MKE) and Korea Institute for Advancement in Technology (KIAT) through the Workforce Development Program in Strategic Technology

References

[1] A. Emadi, S.S. Williamson, J. Power Electron. 1 (2001) 133–144.
[2] F. Urbani, G. Squadrito, O. Barbera, G. Giacoppo, E. Passalacqua, O. Zerbinati, J. Power Sources 169 (2007) 334–337.
[3] F. Dundar, F. Barbir, H. Gorgun, A. Ata, Int. Hydrogen Energy Congr. (2005).
[4] C. Hebling, B. Burger, A. Hakenjos, J. Hesselmann, H. Münter, D. Pocza, J.O. Schumacher, U. Wittstatt, M. Zedda, M. Zobel, The Fuel Cell World 2003 Proceedings in Lucerne, Switzerland, 2003, pp. 143–152.
[5] A.P. Vega-Leal, F.R. Palomo, F. Barragan, J. Power Sources 169 (2007) 194–197.
[6] A.N. Wilhelm, B.W. Surgenor, J.G. Pharoah, IEEE/ASME Trans. Mech. 11 (2006) 471–476.
[7] F.N. Büchi, S. Srinivasan, J. Electrochem. Soc. 144 (1997) 2767–2772.
[8] R. Eckl, W. Zehtner, C. Leu, U. Wagner, J. Power Sources 138 (2004) 137–144.
[9] P. Berg, K. Promislow, J. St.Pierre, J. Stumper, B. Wetton, J. Electrochem. Soc. 151 (2004) A341–A353.
[10] S.U. Jeong, E.A. Cho, H.-J. Kim, T.-H. Lim, I.-H. Oh, S.H. Kim, J. Power Sources 159 (2006) 1089–1094.
[11] J.T. Pukrushpan, A.G. Stefanopoulou, H. Peng, Control of Fuel Cell Power Systems: Principles, Modeling, Analysis and Feedback Design, Springer, 2004, pp. 57–90.
[12] F. Barbir, PEM Fuel Cells: Theory and Practice, Elsevier Academic Press, 2005.
[13] J. Larminie, A. Dicks, Fuel Cell Systems Explained, second ed., John Wiley and Sons, 2003.
[14] F.P. Incropera, D.P. DeWitt, Fundamentals of Heat and Mass Transfer, fifth ed., John Wiley and Sons, 2002, pp. 534–592.
[15] J.P. Bird, Model of the Air System Transients in a Fuel Cell Vehicle, Masters Thesis, Virginia Polytechnic Institute and State University, 2002.
[16] D. Ibrahim, Microcontroller Based Applied Digital Control, John Wiley and Sons, 2006.
[17] NI 6124/6154 User Manual, National Instruments Corporation, 2008.
[18] T.-H. Kim, W. Choi, J. Korean Inst. Power Electron. 13 (2008) 469–475.